

# Zeeman Effect

Alex Povilus  
Physics 441- Fall 2003

December 20, 2003

## Abstract

The Zeeman Effect is observed by application of a strong magnetic field to a mercury vapor cell and exciting transitions by placing a high voltage across the sample. Energy splittings due to change of magnetic field can be measured by passing the light from the 546.07nm transition through a Fabry-Perot Interferometer and measuring interference effects. The difference in energy splitting between the  $6^3P_2$  and  $7^3S_1$  states was found to be linear with wavenumber  $\Delta k = 2.409 \pm 0.037(stat) \pm 0.173(sys) \times 10^{-5} cm^{-1}/gauss$ , or  $\Delta E = 7.617 \pm 0.073(stat) \pm 0.550(sys) \times 10^{-29} J/gauss$ .

## I. Background

The Zeeman effect was historically an important indicator of atomic structure found at the turn of the century by renowned physicist Pieter Zeeman. Zeeman observed in 1896 that sodium's spectral pair of D-lines would split when placed in an intense magnetic field in a laboratory. [1] Working under his mentor Lorentz, Zeeman confirmed Lorentz's model for electron orbitals by constructing a model for his observations in the context of electron angular momentum. In addition, Zeeman was able to demonstrate applications of his method such as measuring the magnetic fields around the sun by observation of spectra at different points on the surface. This model was later modified to fit a quantum mechanical model which utilized an m-state to describe the energy splitting found when placing an atom in a magnetic field.

To better understand this idea, one can consider a magnetic dipole placed into an external magnetic field. The dipole inherently has some magnetic dipole constant,  $\mu$ . Placing the dipole into a magnetic field  $\mathbf{B}$ , we find that the Hamiltonian of the system takes the form,

$$H_\mu = -\mu \cdot \mathbf{B} \quad (1)$$

Extending this idea to atoms, we find that the structure of the atom allows for two distinct electronic magnetic dipole moments. The first moment occurs from the inherent spin of the electron,  $\mu_S$  while the second,  $\mu_L$ , is a result of the orbital motion of the particle about the nucleus, derived from the angular momentum. These two moments can be given in terms of the quantum parameters  $\mathbf{L}$  and  $\mathbf{S}$  as,

$$\mu_S = -\frac{e}{m} \mathbf{S} \quad (2)$$

$$\mu_L = -\frac{e}{2m} \mathbf{L} \quad (3)$$

Thus, through first order-perturbation theory, we can express the energy splitting as,

$$\Delta E = \frac{e}{2m} \mathbf{B} \cdot \langle \mathbf{L} + 2\mathbf{S} \rangle \quad (4)$$

In our experiment, an energy splitting for mercury was observed. However, as an order-of-magnitude estimate, we can calculate this difference of energy for the simplified case of hydrogen. Knowing that  $L_z = \hbar l$ , we find that by the above equation  $\Delta E \approx 10^{-28} J/gauss$  for a  $\Delta m = 0$  transitions. In the analysis of the results, it will be seen that this estimate is in fact very accurate.

More specifically, in this experiment, we actually measure the *difference* of two unequal Zeeman splittings in the  $6^3P_2$  and  $7^3S_1$  states of mercury. This effect occurs from the difference in  $\mathbf{L}$  between the states. Given the discussion above, the prediction can be made that the Zeeman splitting will follow the behavior,

$$\Delta E_{Zeeman, 6^3P_2} = g_0 |\mathbf{B}| \quad (5)$$

$$\Delta E_{Zeeman, 7^3S_1} = g_1 |\mathbf{B}| \quad (6)$$

for some constants  $g_0$  and  $g_1$ . Using a linear polarizer, as discussed later, one can selectively choose to observe  $\Delta m = 0$  transitions only and therefore extrapolate the experimental value of  $g_1 - g_0$ . The observation of a difference in the Zeeman splittings is often called the anomalous Zeeman effect in literature.

## II. Apparatus: Fabry-Perot Interferometer

The apparatus focuses on the ability to read small changes the energy of photons. This can be achieved by employing an interferometer, in general a device which utilizes the interference effects of light to measure small changes in the energy per photon of that light. Such devices are employed in a wide range of applications, from tuning lasers to possible measurement of gravitational waves in the LIGO initiative. In fact, interferometry is not limited to merely photons, but can be achieved with any phase dependent quantum system such as a mass interferometer which can theoretically measure incredibly small changes of acceleration in a system, better than  $10^{-5}m/s^2$ . To observe the Zeeman effect in mercury, however, we concern ourselves primarily with the 546.1 nm,  $7^3S_1 \rightarrow 6^3P_2$  transitions. In this case we employ a Fabry-Perot interferometer to create high-resolution interference patterns suitable for measurement.

The Fabry-Perot interferometer is a special type of interferometer that utilizes two partially reflective glass plates placed closely together with a layer of air between. The glass plates may be coated with a thin layer of silver in order to increase reflectivity between the two plates. These plates, when placed exactly parallel to each other, create interference patterns by reflecting light multiple times within the air cavity. Much care must be taken in aligning the plates properly to acquire useful data; this can be done via the kinematic mount used to hold one of the plates. Ideally, when aligned, the interference pattern should have little dependence on the angle at which one views the image.

The solution for the interference pattern is considered explicitly as a problem in Jackson's *Classical Electrodynamics*. [3] The transmission coefficient can be given as,

$$T = \frac{|\mathbf{E}'_0|}{|\mathbf{E}_0|} = \frac{(4n(\cos(i)/\cos(r)))^2}{(1 + n(\cos(i)/\cos(r)))^4 + (1 - n(\cos(i)/\cos(r)))^4 - 2(1 - n^2(\cos(i)/\cos(r))^2)\cos(2\phi + \phi_0)} \quad (7)$$

where  $\phi$  denotes the change of phase across the air gap,  $i$  is the angle of incidence into the air gap,  $r$  is the refractive angle, and  $n$  is the index of refraction of the glass. Considering a plane wave with  $i = r = 0$ , we arrive at the value,

$$T = \frac{16n^2}{(2 - 2\cos(2\phi + \phi_0))n^4 + (12 + 4\cos(2\phi + \phi_0))n^2 + (2 - 2\cos(2\phi + \phi_0))} \quad (8)$$

for a plane wave with incident phase  $\phi_0$ . The incident phase, geometrically, can be approximated as function of distance from the center of the mercury lamp image. This function reduces to a locally quadratic relation, as discussed in the next section, resulting in the ring pattern with a ring at radius  $\sqrt{m}$  for each integer  $m$ .

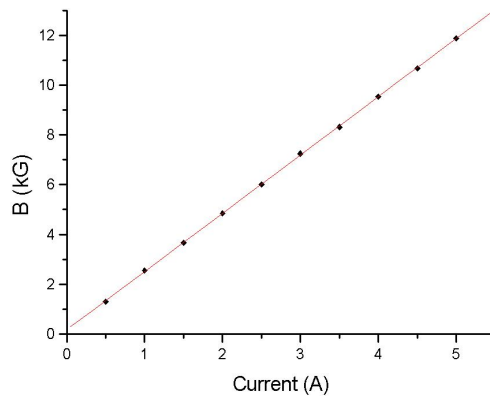


Figure 1: This is a graph of the calibration curve for the magnetic field. The units for magnetic field strength are in kilogauss. Systematic error for measurements include a current uncertainty of 0.2A and a magnetic field uncertainty of 0.03kG.

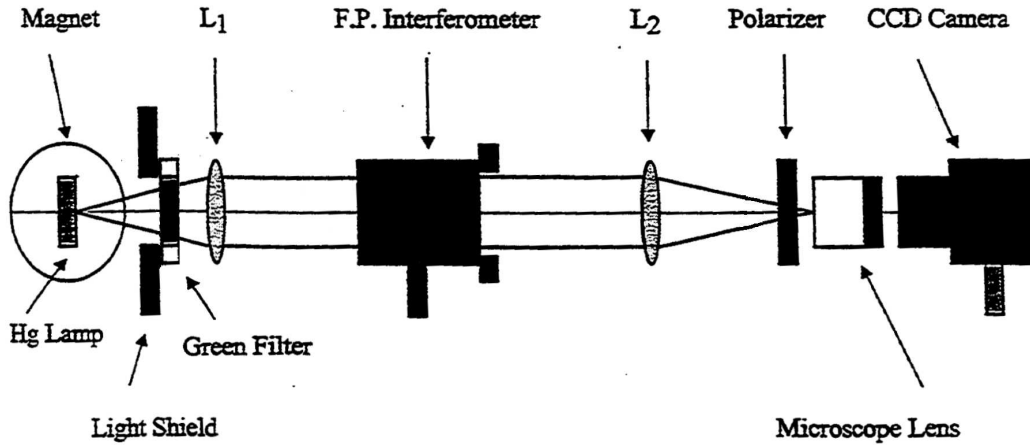


Figure 2: The setup used in this experiment.

### III. Apparatus: Optics and Data Collection

This lab, as mentioned before, analyzes the difference of energy induced in quantum  $m$ -states of mercury by applying an external magnetic field. The lamp is placed between two large sets of coils which produce a magnetic field of up to 1.2 Tesla at the sample. The magnets are controlled via a power supply capable of driving up to 5.3 Amps through the pair of coils simultaneously. This system requires an initial calibration to correlate the input current with the magnetic field (Fig. 1). Measurements were taken of the magnetic field using a Hall effect probe over a range of power supply currents. The field produced by the electromagnet, as expected, was found to be linearly dependent to the current passed through the coil, resulting in the calibration curve,  $|\mathbf{B}| = (0.166 \pm 0.022) + (2.341 \pm 0.007)I$ .

Excitation within the lamp occurs by applying a large voltage across the lamp. In this case, many different mercury transitions are expressed in the output of the lamp. In order to measure any type of interference pattern, it is best to select a nearly monochromatic portion of this spectra for observation. In this case, the 546.07nm green transition was selected for its high intensity and relatively empty spectrum about this wavelength. A green filter is placed in front of the lamp to select only photons near this color. The filtered light passes through a lens, creating a plane wave, and into the Fabry-Perot. Note that by geometry, the wavefronts are parabolically shaped rather than planes due to the extra distance the light must travel to reach the sides of the lens. This is what generates the locally quadratic relation for phase mentioned in the previous section and thus the observable rings on the interferometer. The image from the interferometer is passed through two lenses and finally a polarization filter into the CCD camera.

The polarization of light is important for observation of interference effects since by selection rules

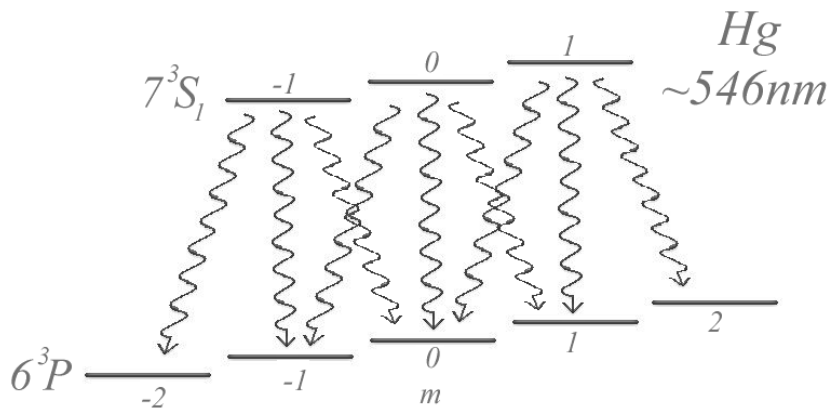


Figure 3: This energy level diagram shows the possible transitions between  $m$  states on the  $7^3S_1 \rightarrow 6^3P_2$  manifold. Note that there are 3 of each  $\Delta m = 0, \pm 1$  transition, giving the nine allowed transitions mentioned in the text.

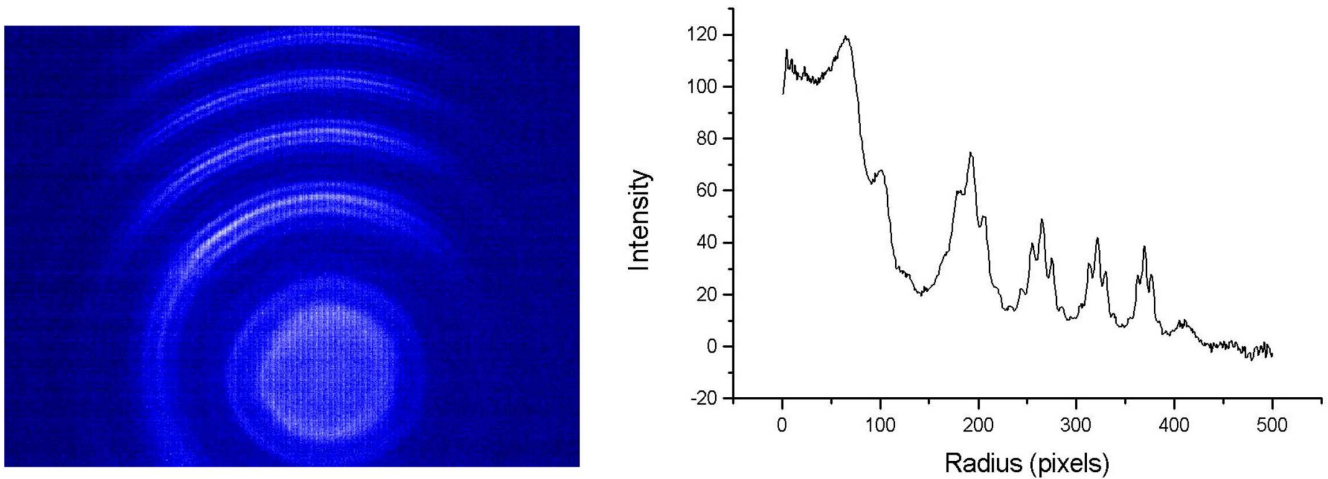


Figure 4: The interference rings, as captured by the CCD camera, are shown on the left. Using the program to calculate radial correlation, we acquire an intensity graph  $S(|\mathbf{r} - \mathbf{r}_0|)$  on the right. The three peaks characterizing the Zeeman splitting are clearly visible in the correlation. The strength of the magnetic field for this measurement was 11880 gauss.

there are nine transitions which make up the 546.07nm spectral line, three of which are  $\Delta m = 0$  and three of each of the  $\Delta m = \pm 1$  transitions (Fig. 3). Linearly polarizing the light in the axis of the magnetic field selects only light from  $\Delta m = 0$  transitions, those that emit linearly polarized photons. Thus, the anomalous Zeeman effect can be observed as the difference in the Zeeman splitting between the  $7^3S_1$  and  $6^3P_2$  m-states.

A CCD camera is used in order to collect data by taking images of the interference rings. The images were acquired through an National Instruments IMAQ-1408 board in a computer and then captured and analyzed in Labview 6.1. The image acquisition was handled by the standard IMAQ drivers included with Labview. Due to the low sensitivity of the CCD camera used, 500 images were taken for each set of rings in order to reduce noise. This effectively integrated the image over approximately 8 seconds, providing a clear image and reducing background noise inherent in most CCD cameras. The images were then processed by a custom program which analyzed the radial correlation of the image, determining the radius of the rings in the image relative to each other. This program loads an image taken from the camera, and allows the user to choose an appropriate center. At this point, the program computes the intensity of the image as a function of radius from the chosen center,  $\mathbf{r}_0$ ,

$$S(|\mathbf{r} - \mathbf{r}_0|) = \frac{\int_{C(|\mathbf{r} - \mathbf{r}_0|)} \text{Img}(\mathbf{r})}{2\pi|\mathbf{r} - \mathbf{r}_0|} \quad (9)$$

where  $\text{Img}(\mathbf{r})$  is the intensity of the image at the point  $\mathbf{r}$  and  $C(|\mathbf{r} - \mathbf{r}_0|)$  is the circle of radius  $|\mathbf{r} - \mathbf{r}_0|$  about the point  $\mathbf{r}_0$ . From this data, the radius of the rings can be extrapolated. A sample of the acquired data is given in Figure 4.

#### IV. Acquired Data

Given the data as seen in Figure 4, preprocessing of data is necessary in order to start in-depth analysis. This involves extracting the radii of the rings from the radial correlation. The Fourier transition can be viewed as a Lorentzian in frequency space, *locally* equivalent to the radial space observed in the graph. Since the rings have a relatively large linewidth on the image, they can not easily be identified by a simple Lorentzian. Using a data analysis program Igor, however, each triplet of rings was fit to a three-Lorentzian function, extrapolating the centroids of all transitions simultaneously. Note that this method does result in a small error since globally the radial space is proportional to the square root of the frequency space. This error should provide a slightly low value of  $\Delta E$  for the inner rings and a high  $\Delta E$  for the outer rings. As an example, the data extracted from Figure 4 is summarized in Table 1. Data was acquired for four sets of data, each at approximately 1200 gauss intervals from 8300 to 11900 gauss. Below this value, the linewidth of each transition is large enough to obscure the distinction between the rings. Thus,  $g_1 - g_0$  was determined by a five separate sets of data for this experiment.

Ring Number	Radius <sup>2</sup> (pixels <sup>2</sup> )				
	a	$\delta_{ab}$	b	$\delta_{bc}$	c
1	31830	5022	36852	5255	42107
$\delta_{12}$	32665		32917		33112
2	64496	5274	69770	5449	75218
$\delta_{23}$	32961		32982		33003
3	97456	5296	102752	5469	108221
$\delta_{34}$	33211		33084		33034
4	130668	5169	135936	5419	141255

Table 1: The table gives the square of the radius of each ring in Figure 4. The ring number gives the set of rings while the labels a, b, and c describe the innermost to outermost rings for each set. The values  $\delta_{ij}$  give the difference in the square radius between the two adjacent i and j rings.

## V. Analysis

Results from Fabry-Perot can be interpreted by knowing the spacing distance between the two reflective surfaces. In this experiment, a spacer was placed between the two surfaces with thickness  $t=2.8 \pm 0.2mm$ . Since the transmission coefficient is dependent upon the value  $2\phi$  (Eq. 8), the difference in wavenumber can be given as,

$$\Delta\nu_{ab} = \frac{\langle \delta_{ab} \rangle}{2t \langle \Delta \rangle} \quad (10)$$

where  $\langle \Delta \rangle$  is the average of the  $\delta_{12}$ ,  $\delta_{23}$ , and  $\delta_{34}$  values in Table 1. The value  $\Delta\nu_{ab}$  can then be transferred to units of energy by the formula,

$$\Delta E = \hbar\omega = \hbar(\Delta\nu_{abc}) \quad (11)$$

For the data in Table 1, this translates into the following set of values:  $\Delta\nu_{ab} = 0.281 \pm 0.006(stat) \pm 0.020(sys)cm^{-1}$ ,  $\Delta\nu_{bc} = 0.292 \pm 0.003(stat) \pm 0.020(sys)cm^{-1}$ . This corresponds to a change of shift in the energy levels equivalent to about  $8.9 \times 10^{-25}J$ .

Having calculated the  $\Delta\nu$  values for each set of magnetic field values, we fit the points to a linear relation in order to evaluate  $g_1 - g_0$ . The data results in a curves of the form,

$$\Delta\nu_{ab} = ((2.376 \pm 0.053(stat) \pm 0.160(sys)) \times 10^{-5}cm^{-1}/gauss)|\mathbf{B}| + (0.003cm^{-1}) \quad (12)$$

$$\Delta\nu_{bc} = ((2.441 \pm 0.053(stat) \pm 0.185(sys)) \times 10^{-5}cm^{-1}/gauss)|\mathbf{B}| + (0.001cm^{-1}) \quad (13)$$

with  $\chi^2_\nu = 0.96, 0.90$  respectively. The results for this are expressed in the graph in Figure 5. Averaging the two slopes above, we arrive at a final figure of  $g_1 - g_0 = (2.409 \pm 0.037(stat) \pm 0.173(sys)) \times 10^{-5}cm^{-1}/gauss$ . This comparable to about half of the expected value of  $\mu_0/hc$ ,  $4.669 \times 10^{-5}cm^{-1}/gauss$ , given in the lab manual.

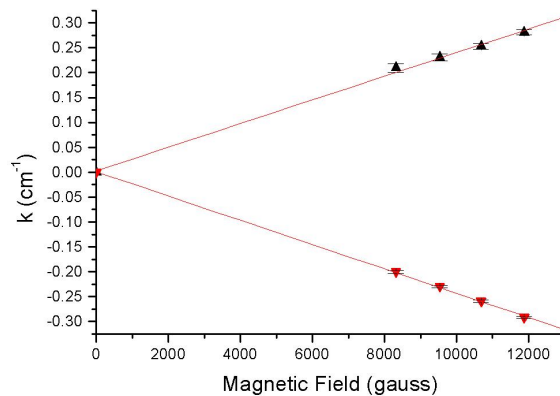


Figure 5: This graph displays the relation between the strength of the magnetic field and both  $\Delta\nu_{ab}$  (upwards triangles) and  $\Delta\nu_{bc}$  (downwards triangles). The equations of each fit line are found in (Eq. 12) and (Eq. 13).

There is a good theoretical reason for this discrepancy involving the electronic spin in the system. In the approximation given in the lab manual, spin of the electrons was not taken into account, leaving the value  $\mathbf{S} = 0$ . In reality, the strength of the spin magnetic dipole is of the same order of magnitude as the angular momentum dipole. The net consideration of both spin and angular dipoles is called the Lande g-factor, given by the equation, [4]

$$g_J(|n, l, s, j \rangle) = 1 + \frac{J(J+1) + S(S+1) - L(L+1)}{2J(J+1)} \quad (14)$$

From this equation, we can make a better approximation for  $g_1 - g_0$  as,

$$g_J(|7, 0, 1, 1 \rangle) - g_J(|6, 1, 1, 2 \rangle) = \left(1 + \frac{2+2-0}{4}\right) - \left(1 + \frac{2+6-2}{12}\right) = 1/2 \quad (15)$$

Thus, we end up with a factor of (1/2) for the difference in the splitting, giving a more acceptable expected value of  $2.335 \times 10^{-5} \text{cm}^{-1}/\text{gauss}$ . This value therefore is well within the bounds of error of the experimental value.

## VI. Error Analysis

Statistical error for this experiment involves two components. The first is the consideration of error when fitting the Lorentzians to the radial correlation of the rings. The error inherent in this measurement is usually much smaller than a pixel ( $< .1$  pixels) and therefore contributed less than 1% since spacing between rings was typically on the order of 10 pixels apart. The second consideration is the error inherent in the calculation of the slope in (Eq.12) and (Eq.13). When summing the average of  $\Delta\nu_{bc}/|\mathbf{B}|$  and  $\Delta\nu_{cb}/|\mathbf{B}|$ , the geometric mean of the errors is taken to be the final statistical error.

Systematic error had a much larger influence in the experimental analysis. Since the uncertainty in the Fabry-Perot thickness was about 7% of the total value, and this value was a final step in the analysis, the total systemic error is somewhat large. This value, in itself, accounts for the small discrepancy between the experimental and actual values. Other, less significant, errors include a persistent noise from the CCD image, despite integration methods, and small perturbations to the image due to lensing effects. The net result is the error given in the previous section.

## VI. Conclusion and Future Improvements

This experiment measured the energy splittings involved with the anomalous Zeeman effect. The value for the difference in the Zeeman splitting between the two energy states was found to be  $\Delta k = 2.409 \pm 0.037(\text{stat}) \pm 0.173(\text{sys}) \times 10^{-5} \text{cm}^{-1}/\text{gauss}$ , or  $\Delta E = 7.693 \pm 0.073(\text{stat}) \pm 0.550(\text{sys}) \times 10^{-29} \text{J}/\text{gauss}$ . This correlated well with the accepted value of  $2.335 \times 10^{-5} \text{cm}^{-1}/\text{gauss}$  once the Lande g-factor of each state was taken into consideration.

Further improvements to this experiment include requiring additional measurements so that the g-factors  $g_0$  and  $g_1$  can be observed directly in this experiment. This would require the measurement of images that are circularly polarized and a few extra calculations using the energy level diagram. In addition, it would also prove useful to use another color filter so that the Zeeman effect can be observed on another possible transition. Finally, a camera with better gain control might prove useful as many of the images in the experiment had relatively weak rings in comparison to the resolution to the camera, requiring such a long integration time.

### References:

- [1] <http://www.nobel.se/physics/laureates/1902/zeeman-bio.html>
- [2] A.C. Melissinos, Experiments in Modern Physics (1966), pp. 43-52, 283-294, and 320-339.
- [3] J.D. Jackson, Classical Electrodynamics (1998), p. 341, Problem 7.3
- [4] D.J. Griffiths, Introduction to Quantum Mechanics (1995), p. 246